

## ARTICLE OPEN



# Modulation of CREB3L2-ATF4 heterodimerization via proteasome inhibition and HRI activation in Alzheimer's disease pathology

Krystal Herline-Killian<sup>1</sup>, Michaela M. Pauers<sup>2</sup>, Jessica E. Lipponen<sup>3</sup>, Michael A. Zrzavy<sup>1</sup>, Cláudio Gouveia Roque<sup>1</sup>, Ethan P. McCurdy<sup>4</sup>, Kyung Min Chung<sup>1</sup> and Ulrich Hengst<sup>1,5</sup>✉

© The Author(s) 2025

Alzheimer's disease (AD) pathology includes transcriptional changes in the neurons, which are in part caused by the heterodimerization of two stress response transcription factors, CREB3L2 and ATF4. We investigated the role of proteasome inhibition and the eIF2 $\alpha$ -kinase HRI in the formation of CREB3L2-ATF4 in neurons exposed to soluble oligomeric A $\beta$ <sub>42</sub>. While HRI activation increased ATF4 expression, it decreased CREB3L2 and CREB3L2-ATF4 levels. Proteasome inhibition, induced by A $\beta$ <sub>42</sub>, leads to increased levels of both transcription factors in the nucleus. These findings suggest that CREB3L2 levels are normally kept low due to rapid degradation, but proteasome inhibition in response to A $\beta$ <sub>42</sub> disrupts this balance, increasing CREB3L2 and heterodimer levels. Activation of HRI not only reduced CREB3L2 and heterodimer levels but also prevented the transcriptional dysregulation of a CREB3L2-ATF4 target, SNX3. Our results suggest that manipulating the HRI pathway during proteasome inhibition could help restore normal gene expression in the context of AD-related protein accumulation.

*Cell Death and Disease* (2025)16:225; <https://doi.org/10.1038/s41419-025-07586-0>

## INTRODUCTION

Alzheimer's disease (AD) is a debilitating neurodegenerative disease characterized among others, by the progressive accumulation of  $\beta$ -amyloid 1-42 (A $\beta$ <sub>42</sub>) and tau protein aggregates, widespread transcriptional changes throughout the brain, and ultimately, profound cognitive deficits [1–3]. Identifying mechanisms driving these transcriptional changes might provide novel targets to therapeutically normalize gene expression in AD [4]. We discovered that a unique heterodimer of two bZIP transcription factors, cyclic AMP-responsive element-binding protein 3-like protein 2 (CREB3L2) and activating transcription factor 4 (ATF4), is present in AD brain [5–7]. This heterodimer is linked to up to 50% of gene expression changes in AD brain, and its induction in neurons is sufficient to elicit AD-typical neuronal changes, including the hyperphosphorylation and secretion of tau, increased A $\beta$ <sub>42</sub> over A $\beta$ <sub>40</sub> production, and disrupted expression of components of the retromer [6], which functions in endosomal-lysosomal trafficking and is defective in AD brain [8, 9]. Most importantly, the prevention of dimer formation rescues neurons from A $\beta$ <sub>42</sub>-induced cell death [6]. CREB3L2-ATF4 is rarely seen in health control brains [6], and the mechanisms governing its formation and or stability specifically in A $\beta$ <sub>42</sub>-exposed neurons or the AD brain remain unknown.

The levels of stress response transcription factors, such as ATF4, are under tight translational control [10]. *Atf4* and *Creb3l2* belong

to a class of mRNAs, whose translation is positively controlled as part of the integrated stress response (ISR) [11]. The ISR is a network of cellular signaling pathways that get activated in response to a variety of stressors to reestablish cellular homeostasis [12]. These pathways converge in the phosphorylation of the  $\alpha$ -subunit of the eukaryotic initiation factor 2 (eIF2 $\alpha$ ) and the resulting synthesis of stress response transcription factors. Currently, it is unclear which of the eIF2 $\alpha$  kinases (PERK, PKR, GCN2, HRI) are activated in response to A $\beta$ <sub>42</sub> in neurons and required for the synthesis and subsequent dimerization of ATF4 and CREB3L2. There is a paucity of data on the role of the ISR kinase HRI in the brain because it was once thought to only function in balancing globin synthesis with heme levels in red blood cells during hemoglobin synthesis [13]. More recently, HRI has received renewed interest as the ISR kinase responsible for phosphorylating eIF2 $\alpha$  during proteasome inhibition [14–17]. Furthermore, HRI has now been identified in the brain and functions in spine growth, memory consolidation, and postsynaptic activity [18, 19]. In addition to translation control, post-translational mechanisms, especially ubiquitination and proteasomal degradation, control the abundance of ATF4 and CREB3L2. ATF4 contains a  $\beta$ -TrCP degron, which unless multiphosphorylated causes its rapid degradation [20]. Similarly, CREB3L2 is rapidly ubiquitinated and degraded by the proteasome under non-stress

<sup>1</sup>The Taub Institute for Research on Alzheimer's Disease and the Aging Brain, Vagelos College of Physicians and Surgeons, Columbia University, New York, NY, USA. <sup>2</sup>Doctoral Program in Neurobiology and Behavior, Columbia University, New York, NY, USA. <sup>3</sup>Graduate Program in Pathobiology and Mechanisms of Disease, Vagelos College of Physicians and Surgeons, Columbia University, New York, NY, USA. <sup>4</sup>Integrated Program in Cellular, Molecular and Biomedical Studies, Vagelos College of Physicians and Surgeons, Columbia University, New York, NY, USA. <sup>5</sup>Department of Pathology & Cell Biology, Vagelos College of Physicians and Surgeons, Columbia University, New York, NY, USA.

✉email: [uh2112@cumc.columbia.edu](mailto:uh2112@cumc.columbia.edu)

Edited by Alexei Verkhratsky

Received: 19 December 2024 Revised: 8 March 2025 Accepted: 21 March 2025

Published online: 31 March 2025

conditions [21]. How these two regulatory mechanisms, translational activation downstream of eIF2 $\alpha$  and ubiquitin-dependent proteasomal degradation, affect the formation and abundance of the CREB3L2-ATF4 heterodimer in A $\beta_{42}$ -exposed neurons remains unexplored.

Here, we report that activation of the ISR is not sufficient for the formation of the CREB3L2-ATF4 but that concurrent inhibition of the cytoplasmic proteasome is required as well. Activation of HRI, which can be activated in response to inhibition of the proteasome, strongly induces ATF4 levels, but its prolonged activation reduced CREB3L2 expression. Consequently, we find that sustained HRI activation prevents heterodimer formation and signaling.

## MATERIALS AND METHODS

### Primary culture of rat embryonic neurons

Timed-pregnant Sprague-Dawley rats were housed in the barrier facility at the Columbia University Institute of Comparative Medicine. All animal procedures were approved by the Institutional Animal Care and Use Committee at Columbia University. Primary cortical neurons were harvested from E15-E18 rat embryos and cell dissociation was performed by incubating with TrypLE Express Enzyme (Thermo Fisher Scientific) for 15 minutes in a water bath at 37°C followed by repeated pipetting through a fine pipette tip. Neurons were plated on substrates coated with 0.1 mg ml<sup>-1</sup> poly-D-lysine (MilliporeSigma) and 2 mg ml<sup>-1</sup> laminin (Bio-Techne) and then grown in Neurobasal medium supplemented with 10% fetal bovine serum (heat inactivated, certified One Shot FBS; Thermo Fisher Scientific), 2 mM L-glutamine (Gibco), 1 mM sodium pyruvate (Gibco), and 50 U ml<sup>-1</sup> penicillin-streptomycin (Gibco) and placed in a humidified atmosphere of 5% CO<sub>2</sub> at 37°C. The next day, the medium was changed to Neurobasal containing 1x B27 (Gibco) and 2 mM L-glutamine. Half-medium changes were performed every 3-4 days and maintained in a 37°C, 5% CO<sub>2</sub> humidified atmosphere until DIV7-8.

### Cell culture

HEK293T (ATCC) were cultured in DMEM supplemented with 10% FBS and 2 mM L-glutamine in a humidified atmosphere of 5% CO<sub>2</sub> at 37 °C. Cells were passaged at 80–95% confluency. Experiments were performed when cells were at a 75-85% confluency.

### Lentivirus constructs, preparation, and transduction

Lentivirus expression plasmids shControl and shHRI (shHRI sequence: 5'-TGCTGTTGACAGTGAGCGCCAAGACAGAGTCCCATTC AATAGTGAA GCCACAGATGATTGAATGGGAACCTGTCTTGTTCCTACTGCCTCGGA-3') were obtained from transOMIC technologies. The original mCMV promoter was replaced with the human ubiquitin C (hUbc) promoter for expression in primary neurons using the In-Fusion HD Cloning Plus kit (Takara Bio). Lentiviruses were produced by transfecting HEK293T cells plated in a 100-mm plate at 85–90% confluency with the lentiviral plasmid and packaging plasmids (pCMV $\Delta$  R8.9 and pHCMV VSVg) using Lipofectamine 3000 transfection reagent (Thermo Fisher Scientific). Cells were changed into neuronal growth medium after 12–16 h. Virus containing medium was passed through a 0.45  $\mu$ m PES filter 33–36 h later, aliquoted, and stored at –80°C. Titters for every batch were determined using a qPCR lentivirus titration kit (Applied Biological Materials). Primary cortical neurons were infected on DIV1 with shHRI or shControl at an MOI 20. Experiments were performed on DIV8 unless indicated otherwise.

### Generation of GFP-tagged CREB3L2

cDNA containing *H. sapiens* CREB3L2 open reading frame was acquired from Genecopoeia (NCBI Reference sequence: NM\_194071; product #EX-H2495-M01) and subcloned into pEGFP-C1 (Clontech). EcoRI and BamHI restriction sites were introduced by PCR with CloneAmp HiFi polymerase (Takara), and end products were validated by Sanger sequencing. In-fusion cloning was used to mutate the S1P cleavage site (In-Fusion HD EcoDry Cloning Kit, Takara).

### A $\beta_{42}$ peptide oligomerization

Lyophilized synthetic A $\beta_{42}$  peptides (Bachem, H-1368) were dissolved to 1 mM in ice-cold 100% 1,1,1,3,3,3-hexafluoro-2-propanol (MilliporeSigma)

by multiple rounds of pipetting, aliquoted, and spun in SpeedVac (Savant Instruments) for 30 minutes. The peptide films were resuspended in dimethyl sulfoxide (DMSO; MilliporeSigma) and further diluted with Ham's F12 medium (Thermo Fisher Scientific), and incubated overnight at 4 °C, as described previously [22]. A $\beta$  was added to dissociated cultures at a concentration of 250 to 750 nM to accommodate batch-to-batch variations. Vehicle controls consisted of a DMSO/F12 mixture, which was similarly incubated overnight.

### Drug treatments

HEK293T and cortical neurons were treated with 1.27  $\mu$ M thapsigargin (MilliporeSigma), 12  $\mu$ M BtdCPU (EMDMillipore), 15  $\mu$ M nelfinavir (MilliporeSigma), 6.8  $\mu$ M bortezomib (MilliporeSigma), or DMSO as a control for 5 h, unless otherwise stated.

### Nuclear fractionation

For nuclear fractionation, cells were plated in 100 mm or 60 mm tissue cultured plates. For collecting a nuclear enriched fraction from A $\beta_{42}$ - or drug-treated samples, cells were washed in HBSS and collected in ice-cold HBSS supplemented with Pierce protease inhibitors (Thermo Fisher Scientific). Samples were collected into pre-chilled microcentrifuges tubes by scraping. Cells were spun at 3,000 RPM for 5 minutes at 4°C. Supernatant was discarded, and the pellets were gently suspended in 200  $\mu$ l hypotonic buffer (20 mM Tris-HCl, pH 6.8, 10 mM NaCl, 5 mM EDTA) supplemented with HALT protease and phosphatase inhibitor cocktail (Thermo Fisher Scientific), by gently pipetting up and down several times. Samples were incubated on ice for 15 minutes and then transferred to a new pre-chilled microcentrifuge tube. 15  $\mu$ l of a 10% Triton-X solution was added to the cells, immediately vortexed for 10 seconds, and then spun down for 10 minutes at 10,000 RPM at 4 °C. The supernatant was collected as the cytoplasmic enriched fraction. The pellet-containing nuclei were suspended in 30  $\mu$ l RIPA buffer (Thermo Fisher Scientific) supplemented with HALT phosphatase and protease inhibitor cocktail (Thermo Fisher Scientific) and incubated for 30 minutes on ice with vortexing every 10 minutes. Samples were centrifuged at 14,000 RPM for 30 minutes at 4 °C and the supernatant containing the nuclear fraction was collected and protein concentration was measured by BCA protein assay.

### Coimmunoprecipitation in primary neuronal culture

Protein A magnetic beads (New England Biolabs) were washed three times in RIPA buffer (Thermo Fisher Scientific). 1  $\mu$ g of monoclonal antibody ATF4 (D4B8, Cell Signaling Technology) and IgG (DA1E, mAb IgG XP<sup>®</sup> Isotype Control) diluted in RIPA buffer was added to 40  $\mu$ l of beads for each condition, mixed for 2 h at 4 °C, and washed three times with RIPA. Antibodies were covalently cross-linked to the protein A beads using bis(sulfosuccinimidyl)suberate (BS3; Thermo Fisher Scientific). During this step, neurons were freshly lysed with RIPA buffer and the resulting protein was quantified by BCA assay. Equal amounts of antibody-bead conjugates were mixed with 500  $\mu$ g lysates overnight at 4 °C with constant rotation. Beads were washed three times at 4 °C with RIPA buffer. Immunoprecipitates were eluted in 50  $\mu$ l of 0.2 M glycine buffer (pH 2.5) and allowed to react for 5 minutes at 4 °C with rotation after a short vortexing step. Eluates were transferred to a new tube, and the elution protocol was repeated. Pooled eluates were neutralized by the addition of 20  $\mu$ l of 1 M Tris-Cl (pH 9.0). An aliquot of eluate was then mixed with 4x Laemmli buffer to be analyzed by western blot and the remainder was immediately stored at –20 °C. CREB3L2 levels were quantified by immunoblot using anti-CREB3L2 antibodies (HPA015068, Atlas Antibodies).

### Immunoblotting

Cells were washed with ice-cold HBSS, scraped, and collected in ice-cold RIPA buffer supplemented with HALT protease and phosphatase inhibitor cocktail. Extracts underwent end-over-end rotation at 4 °C for 30 minutes, followed by centrifugation at 14,000 RPM for 30 minutes at 4 °C. Supernatants were collected, and protein concentration was measured using BCA assay (Pierce). Lysates were mixed in Laemmli sample buffer (Biorad) containing 100 mM dithiothreitol (DTT) and heated to 95 °C for 5 minutes. Samples were resolved by SDS-PAGE using NuPage MOPS SDS buffer and NuPAGE electrophoresis system (Thermo Fisher Scientific), followed by wet transfer using the XCell II Blot Module (Thermo Fisher Scientific) to 0.2  $\mu$ m pore-sized nitrocellulose membranes (GE Healthcare). Membranes were blocked for 1 h with 5% milk in TBS containing 0.1% Tween (TBST) and washed in TBST. Nitrocellulose membranes blotted

overnight at 4°C using the following primary antibodies: anti-CREB3L2 (1:1000; HPA015068, Atlas Antibodies), CREB3L2 (1:1000; MABE1018, MilliporeSigma), anti-ATF4 (1:1000; #11815, Cell Signaling Technology), anti-SNX3 (1:1000; ab56078, Abcam), anti-S2P (1:1000; AB140594, Abcam), anti- $\beta$ -actin (1:10,000; #3700, Cell Signaling Technology), and anti-HDAC1 (1:10,000; ab109411, Abcam). The next day, membranes were washed with TBST, and incubated with IgG anti-mouse or anti-rabbit, HRP secondary antibodies (Thermo Fisher Scientific) for 1 h at room temperature. Membranes were washed, and signals were visualized on KwikQuant Imager (Kindle Biosciences) using 1-Shot Digital-ECL Substrate Solution (Kindle Biosciences) and quantified using Fiji/ImageJ. Replicates for an experiment were always run in a random order on each blot to minimize position effects. Full length, uncropped original western blot s are available as a Supplementary File.

### Proximity ligation assays and subsequent quantification

Cells grown on glass-bottom dishes (MatTek Corporation) were washed 3x with PBS fixed in 4% paraformaldehyde and 4% sucrose in PBS (pH 7.4) for 15 minutes at room temperature. After PBS washes, neurons were permeabilized with 0.2% Triton X-100 in PBS for 10 minutes. Blocking was performed for 1 h with 5% heat-inactivated goat serum (Gibco) diluted in PBS, and primary antibodies (rabbit anti-CREB3L2, 1:300, HPA015534 (Atlas antibodies); mouse anti-ATF4, 1:300, 2B3 WH0000468M1 (MilliporeSigma)), were prepared in blocking solution and then incubated overnight at 4°C. PLA protocol was performed using Duolink In situ Red Detection reagents (MilliporeSigma) with TBS and TBST. All incubations were performed in a humidity chamber and in a hybridization oven (Hoefer Red Roller II). After the last wash step of the Duolink protocol, neurons were counterstained with Alexa Fluor 488-conjugated  $\beta$ III-tubulin antibody (1:500; BioLegend) diluted in a 1% TBS for 1 h and preserved in Duolink In Situ Mounting Medium with DAPI (MilliporeSigma). Samples were imaged using an Axio Observer Z1 microscope (Zeiss) on 63x oil objective and Zen Blue 2.1 software (Zeiss) or, when visualizing nuclear events, using an Andor BC43 benchtop confocal microscope on 60x oil objective and Fusion software with subsequent image processing in ImarisViewer. Imaging settings were kept constant between conditions. PLA puncta for CREB3L2-ATF4 were counted manually for nuclear events or, for total somatic events, quantified using the published speckle counting pipeline from the cell imaging analysis software CellProfiler [23]. When quantifying total somatic events, puncta were normalized to the area of soma, which had been manually traced using the IdentifyObjects-Manually module in a blinded fashion.

### Proteasome assay

Previously collected A $\beta_{42}$ - or vehicle-treated neurons stored at -80 °C were thawed on ice. Cells were lysed in a lysis buffer (50 mM HEPES, 10 mM NaCl, 1.5 mM MgCl<sub>2</sub>, 1 mM EDTA, 0.5% Triton X) supplemented with 2 mM ATP, and resulting lysates were collected and stored on ice. Equal volumes of lysate were added to assay buffer (50 mM HEPES, 10 mM NaCl, 1.5 mM MgCl<sub>2</sub>, 1 mM EDTA, 2 mM ATP, 5 mM DTT, and 10 mM of a fluorogenic substrate [Suc-LLVY-AMC (Enzo Life Sciences), Z-ARR-AMC (EMD Millipore), or Z-LLE-AMC (EMD Millipore)] in 96-well black/clear bottom plates (Thermo Fisher Scientific). For the assay buffer, ATP, DTT, and the fluorogenic substrate were added fresh. Conditions were performed in duplicates. All samples were assayed with and without proteasome inhibitor (bortezomib or epoxomicin (Enzo Life Sciences)) to determine background AMC cleavage by other proteases in the sample. Plates were kept in the dark at 37 °C for 2 h then read at Ex/Em = 350/460 nm on a fluorescent plate reader (Tecan). Proteasome activity was determined for a single sample by subtracting the relative fluorescence of a bortezomib/epoxomicin treated sample from that of the same sample not treated with inhibitor.

### Statistical analysis

Statistical analysis was performed using GraphPad Prism 10.4.0. When comparing the means of two groups, a paired or unpaired *t*-test was performed depending on the experimental design (see figure legends). When comparing the means of three independent groups, a one-way analysis of variance (ANOVA) followed by Dunnett's multiple comparisons test or Tukey's multiple comparisons test was performed depending on the experimental design. When comparing the means of multiple groups encompassing two independent variables, two-way ANOVA with Holm-Šidák multiple comparison tests were performed. A number of biological replicates is indicated in each figure legend.

## RESULTS

### ER stress alone is insufficient to induce CREB3L2-ATF4 heterodimerization in neurons

The AD-linked peptide soluble oligomeric A $\beta_{42}$  induces the formation of a pathogenic heterodimer between the stress response transcription factors CREB3L2 and ATF4 in neurons [6], but the mechanisms controlling their expression and heterodimerization remain unclear. Upon activation of the ISR, eIF2 $\alpha$ -phosphorylation selectively increases the translation of mRNAs containing an upstream open reading frame (uORF) in their 5'-untranslated region (UTR), such as *Atf4* [24]. CREB3L2 belongs to the OASIS family of ER stress transducers, whose expression is translationally controlled by cellular stress [11, 25]. Despite being an OASIS family member, being translated in response to ER stress, and containing several conserved potential uORFs in its 5'UTR (Fig. 1A), *Creb3l2* mRNA has not yet been formally identified as an effector of the ISR. Induction of ER stress by treating cortical neurons with the sarcoplasmic and endoplasmic reticulum Ca<sup>2+</sup>-ATPase (SERCA) inhibitor thapsigargin resulted in a marked increase in CREB3L2 expression as determined by immunoblot, which was abolished by transfecting the neurons with an siRNA targeting *Creb3l2* or by treating the neurons with GSK2606414, a selective PERK inhibitor [26] (Fig. 1B). This formal confirmation that both *Atf4* and *Creb3l2* are ISR effector mRNAs, prompted us to identify the eIF2 $\alpha$  kinase(s) involved.

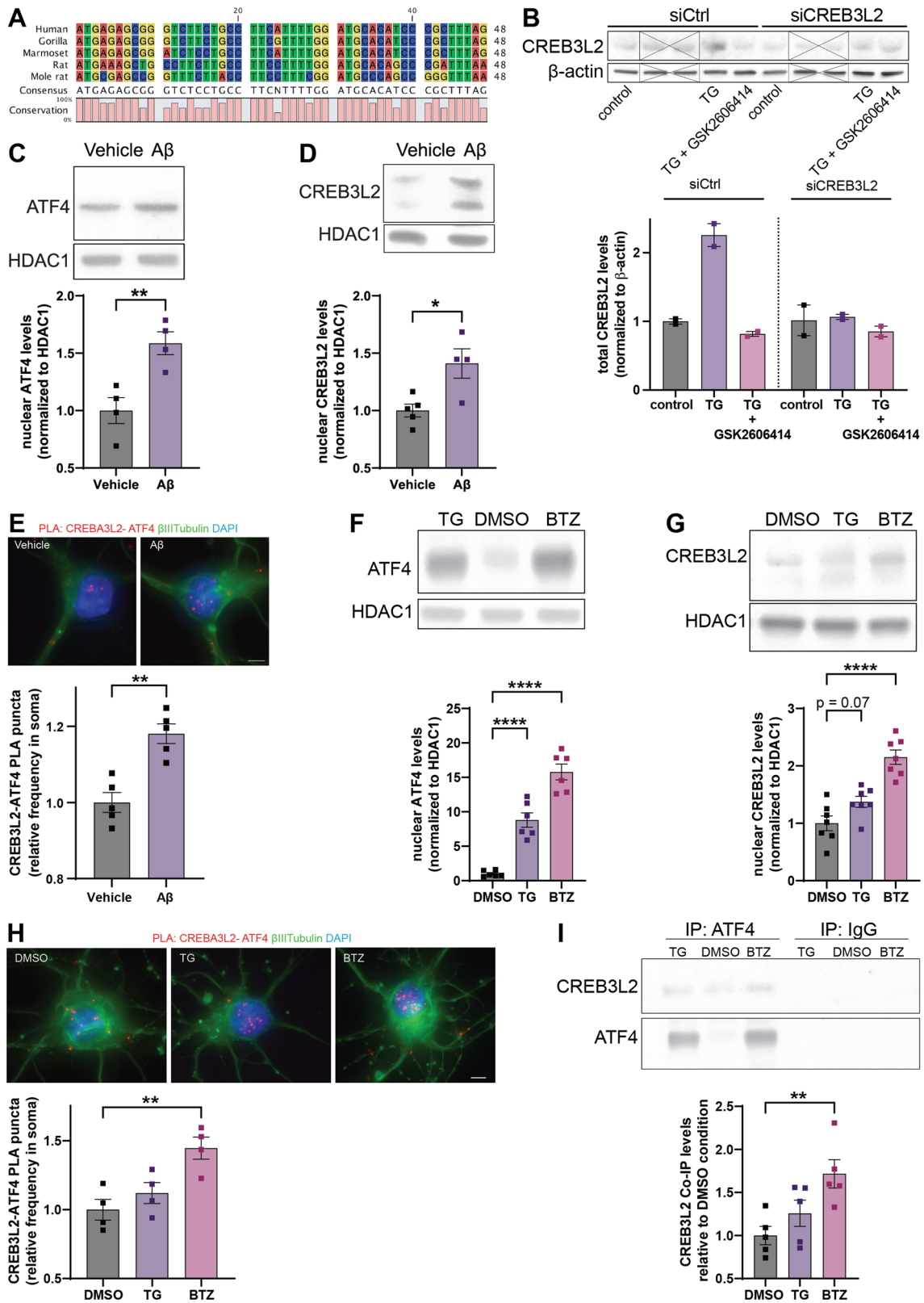
We treated cortical neurons for 36 h with soluble oligomeric A $\beta_{42}$  and determined the levels of ATF4 and CREB3L2 nuclear lysates by immunoblotting. A $\beta_{42}$  induced a significant increase for both transcription factors in neuronal nuclei (Fig. 1C, D), as well as a marked increase in CREB3L2-ATF4 heterodimers as detected by proximity ligation assay (PLA) (Fig. 1E). To test whether ER stress was similarly sufficient to induce CREB3L2-ATF4 signaling, we treated primary cortical neurons with thapsigargin for 5 h. Nuclear ATF4 levels were induced to a much greater extent than with A $\beta_{42}$ -treatment, while the induction of ER stress failed to cause a significant increase in CREB3L2 levels (Fig. 1F, G). Because heterodimer formation is not necessarily driven by changes in the protein levels, we investigated if induction of ER stress would lead to an increase in CREB3L2-ATF4 heterodimers, even in the absence of CREB3L2 upregulation. With two complementary approaches, proximity ligation assay (PLA) and co-immunoprecipitation (co-IP), we did not detect any induction of CREB3L2-ATF4 dimerization in response to thapsigargin (Fig. 1H, I).

### Proteasome inhibition triggers CREB3L2-ATF4 heterodimerization

CREB3L2 and ATF4 are also known to be affected by the inhibition of the proteasome [11, 21, 27], and indeed, proteasome inhibition with bortezomib (BTZ) for 5 h led to an increase in both ATF4 and CREB3L2 protein levels (Fig. 1F, G). Levels of the heterodimer complex were also increased upon BTZ treatment as visualized by PLA and co-IP (Fig. 1H, I), indicating that an increase in CREB3L2-ATF4 heterodimer levels requires proteasome inhibition. In AD, proteasome activity is impaired [28–30], and A $\beta_{42}$  inhibits the activity of the proteasome [29, 31–36]. To determine if extracellular soluble oligomeric A $\beta_{42}$  in our experimental system inhibited the proteasome, we measured chymotrypsin-, trypsin, and caspase-like activity of the proteasome and confirmed that proteasome activity was significantly reduced in neurons treated with A $\beta_{42}$  (Fig. 2).

### A $\beta_{42}$ induces S2P-dependent cleavage of CREB3L2

The formation and function of CREB3L2-ATF4 heterodimers requires several distinct steps, including the synthesis (and in the case of CRB3L2 processing) of both transcription factors, their binding, and the translocation of the heterodimer into the nucleus. CREB3L2 is produced as a transcriptionally inactive ER-transmembrane protein that can translocate to the nucleus only



after being processed by the ER membrane-bound site-1 and/or site-2 proteases, S1P and S2P, respectively [11]. Previously, we reported that the proteolytic cleavage of CREB3L2 and its subsequent release from the ER membrane are dependent on S2P in dorsal root ganglion neurons [37]. To confirm that S2P

cleavage alone is sufficient to release CREB3L2 from the ER membrane in other cells as well, we transfected HEK293 cells with GFP-CREB3L2 carrying a mutated S1P site and then co-expressed cells with S2P. GFP signals were originally reticular in nature (membrane-bound, full-length CREB3L2) but distinctively

**Fig. 1 Proteasome inhibition induces formation of CREB3L2-ATF4 complexes in neurons.** **A** The 5' uORF of CREB3L2 is conserved across various higher order vertebrates. **B** Induction of ER stress causes PERK-dependent CREB3L2 synthesis. Cortical neurons were cultured for 10 DIV and treated with thapsigargin (1  $\mu$ M) and/or GSK2606414 (5  $\mu$ M) for 5 h. Scrambled control or CREB3L2-targeting siRNA was applied for 36 h before treatments.  $n = 2$  replicates; unrelated lanes crossed out. **C-D** Immunoblot analysis of nuclear ATF4 (**C**) and CREB3L2 (**D**) levels in cortical neurons treated with vehicle or  $A\beta_{42}$  for 36 h. Means  $\pm$  SEM of  $n = 4-5$  independent biological replicates, normalized to HDAC1 expression;  $*p = 0.0153$ ,  $**p = 0.0082$ , unpaired t-test. **E** PLA for CREB3L2-ATF4 in cortical neurons treated with  $A\beta_{42}$  for 8 h. Means of means  $\pm$  SEM of  $n = 5$  independent biological replicates, 48-50 optical fields per condition. Number of puncta normalized to area of neuronal soma. Unpaired, two-tailed t-test.  $**p < 0.01$ . Scale bar, 5  $\mu$ m. **F-G** Immunoblot analyses of ATF4 (**F**) and CREB3L2 (**G**) levels in nuclear lysates of vehicle (DMSO), thapsigargin (TG), or bortezomib (BTZ) treated cortical neurons. Means  $\pm$  SEM of  $n = 7$  independent biological replicates, normalized to HDAC1. One-way ANOVA followed by Dunnett's multiple comparison test.  $****p < 0.0001$ . **H** PLA of CREB3L2-ATF4 in cortical neurons treated with vehicle (DMSO), bortezomib (BTZ), or thapsigargin (TG) for 5 h. Means of means  $\pm$  SEM of  $n = 4$  independent biological replicates, 40 optical fields per condition. Number of puncta normalized to area of neuronal soma. One-way ANOVA followed by Dunnett's multiple comparison test.  $*p < 0.05$ . Scale bar, 5  $\mu$ m. **I** Co-immunoprecipitation of CREB3L2 with anti-ATF4 antibodies or control IgG from lysates of cortical neurons treated with vehicle (DMSO), thapsigargin (TG), or bortezomib (BTZ) for 5 h. Means  $\pm$  SEM of  $n = 5$  independent biological replicates. One-way ANOVA followed by Dunnett's multiple comparison test.  $**p < 0.001$ .

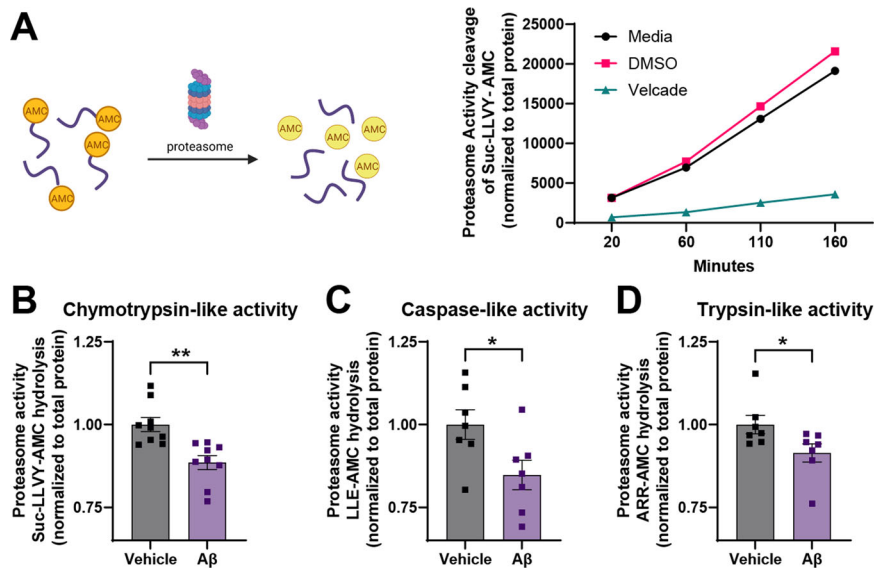


**Fig. 2 Soluble oligomeric  $A\beta_{42}$  causes reduced proteasome activity in neurons.** **A** Validation of the proteasome activity assay. Proteasome activity assays on lysates of cortical neurons treated with vehicle or  $A\beta_{42}$  for 8 hours. Peptidase activity of the 20S proteasome was measured at 120 minutes using specific fluorogenic substrates (50  $\mu$ M): Suc-LLVY-AMC (chymotrypsin-like; **B**), Z-LLE-AMC (caspase-like; **C**), or Z-ARR-AMC (trypsin-like; **D**). Means  $\pm$  SEM of  $n = 7$  (**B**) or 9 (**C**, **D**) independent biological replicates. Unpaired, two-tailed t-tests.  $*p < 0.05$ ;  $**p < 0.01$ .

accumulated in the nucleus with S2P co-expression, indicating that cleavage and activation can occur independently of S1P (Fig. 3A). Likewise, immunoblot analysis demonstrated that expression of S2P, but not S1P, was sufficient to promote the cleavage of CREB3L2 while mutating the S1P cleavage site did not impede its processing, indicating that CREB3L2 activation can occur independently of S1P (Fig. 3B). To investigate the necessity of S2P for the cleavage of endogenous CREB3L2, we used a pharmacological inhibitor of S2P, nelfinavir (NF) [37, 38]. In HEK293 cells, levels of cleaved CREB3L2 were increased by thapsigargin-induced ER stress and proteasome inhibition and treatment with NF abolished this effect (Fig. 3C). Likewise, in HEK293 cells expressing HRP-tagged full-length CREB3L2, the  $A\beta_{42}$ -induced cleavage of CREB3L2 was reduced in the presence of NF (Fig. 3D). Additionally, treatment with NF prevented the  $A\beta_{42}$ -induced nuclear localization of CREB3L2 in cortical neurons (Fig. 3E). Together, these data establish that S2P activity is necessary for the nuclear accumulation of CREB3L2 in response to  $A\beta_{42}$  exposure.

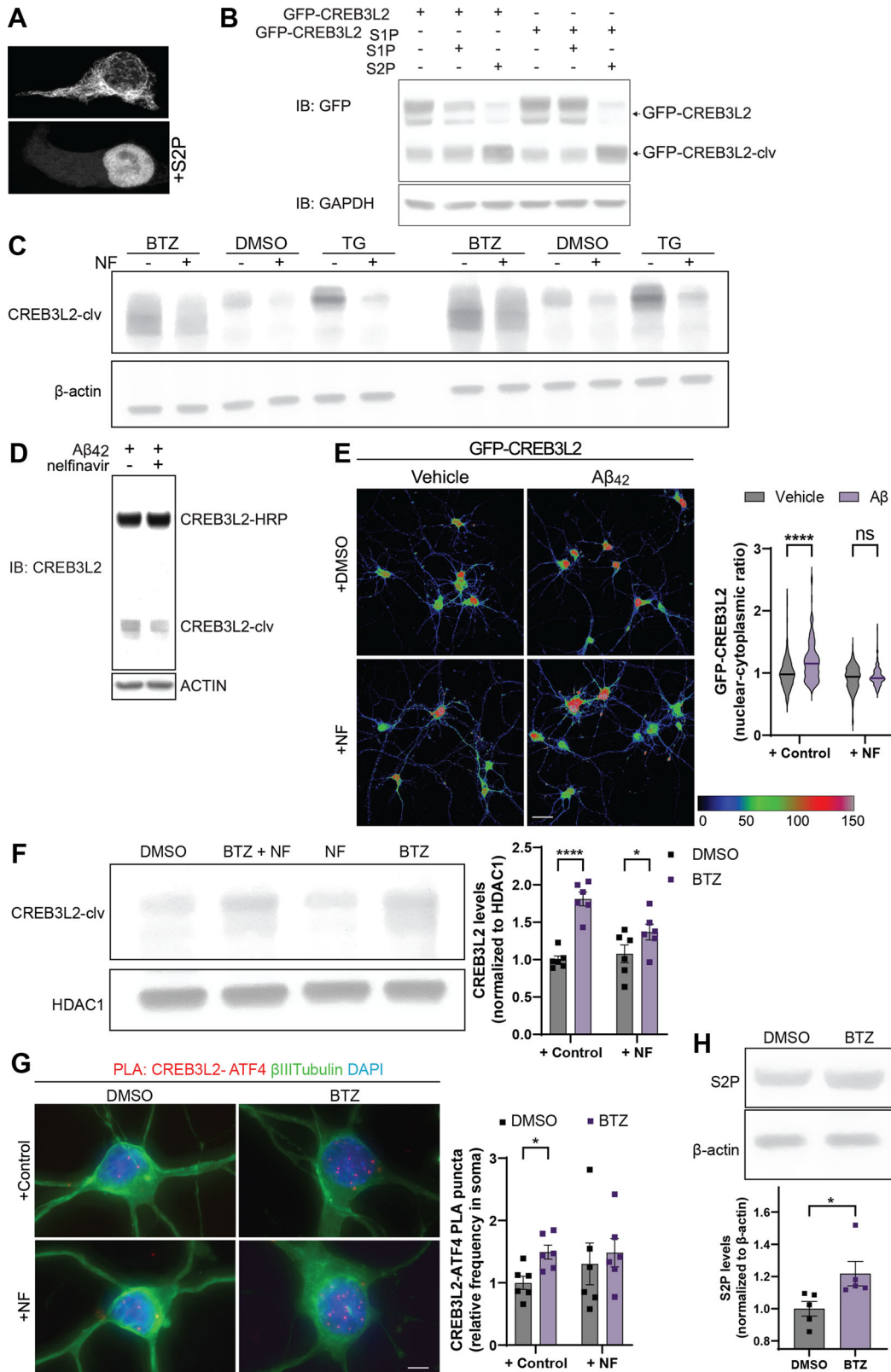
#### Inhibition of the proteasome induces cleavage of CREB3L2 by S2P

To investigate the effects of proteasome inhibition on the subcellular localization of cleaved CREB3L2, we treated neurons

with BTZ for 5 h in the presence of NF. The proteasome inhibitor-dependent increase in nuclear CREB3L2 levels was greatly reduced by S2P inhibition (Fig. 3F). NF did not prevent the BTZ-dependent accumulation of CREB3L2-ATF4 heterodimers in neurons, reflecting that S2P-dependent cleavage is not required for dimerization of the transcription factors, just for the localization to the nucleus (Fig. 3G). Next, we analyzed levels of S2P to determine if proteasome inhibition in neurons could contribute to the increased cleaved levels of CREB3L2, and indeed, S2P levels were increased by proteasome inhibition (Fig. 3H). Together, these data establish that proteasome inhibition increases S2P-dependent cleavage of CREB3L2, potentially by increasing the expression S2P.

#### CREB3L2 levels are negatively regulated by HRI activation

So far, our data indicated that proteasome inhibition is crucial for CREB3L2-ATF4 signaling, but the eIF2 $\alpha$  kinase controlling translation of *Atf4* and *Creb3l2* remained unidentified. Proteasome inhibition activates HRI-eIF2 $\alpha$  signaling [14, 16], and HRI is activated in the presence of amyloid-like protein aggregates and by  $\alpha$ -synuclein in non-neuronal cells [39, 40]. To determine the role of HRI activity in regulating levels of ATF4 and CREB3L2 in neurons, we treated cortical neurons with a small molecule



activator of HRI, BtdCPU [41]. Treatment with BtdCPU resulted in significantly increased ATF4, but a statistically non-significant decrease in CREB3L2 levels in whole cell lysates (Fig. 4A). To ensure that any effect seen with BtdCPU was mediated by HRI, we transduced cortical neurons with virus expressing non-

targeting control or HRI-targeting shRNAs (shCtrl and shHRI, respectively). The increase in ATF4 levels observed with BtdCPU treatment was abolished in shHRI neurons (Fig. 4B). To gain further insight into the role of HRI in regulating the transcriptionally relevant cleaved form of CREB3L2, we analyzed

**Fig. 3 Proteasome inhibition activates S2P-dependent cleavage and nuclear localization of CREB3L2.** **A** Subcellular distribution of a GFP-CREB3L2<sub>S1P</sub> (full-length) fusion protein carrying a mutated S1P cleavage site with or without S2P co-expression in HEK293 cells. Scale bar, 25  $\mu$ m. **B** Immunoblot analysis for full-length and cleaved (clv) GFP-CREB3L2 or GFP-CREB3L2<sub>S1P</sub> in HEK293 cells expressing either S1P or S2P. **C** Immunoblot analysis of endogenous CREB3L2 processing in HEK293 cells treated with vehicle (DMSO), thapsigargin (TG), or bortezomib (BTZ) for 5 h; shown are  $n = 2$  independent biological replicates. **D** Immunoblot analysis of HRP-tagged, full-length CREB3L2 processing in HEK293 cells treated with A $\beta$ <sub>42</sub> in the presence of vehicle or nelfinavir (NF) for 2 h. **E** Quantitative immunofluorescence imaging of cortical neurons expressing full-length GFP-CREB3L2 incubated with A $\beta$ <sub>42</sub> or vehicle (2 h). Cells were pre-treated for 30 minutes with NF or control before A $\beta$ <sub>42</sub> stimulation. Nuclear-to-cytoplasmic GFP fluorescence ratios are presented as means  $\pm$  SEM of 138–161 neurons per condition, obtained over  $n = 3$  independent biological replicates. Holm-Šídák multiple unpaired t-tests, \*\*\*\* $p$ -value < 0.000001. Scale bar, 25  $\mu$ m. **F** Immunoblot analysis of nuclear CREB3L2 and ATF4 levels in cortical neurons treated with vehicle (DMSO) or bortezomib (BTZ) in the presence or absence of nelfinavir (NF). Means  $\pm$  SEM of  $n = 6$  independent biological replicates, normalized to HDAC1. Holm-Šídák multiple unpaired t-tests, \*\*\*\* $p$  < 0.0001; \* $p$  < 0.05. **G** PLA of CREB3L2-ATF4 in cortical neurons treated with vehicle (DMSO) or bortezomib (BTZ) in the presence or absence of nelfinavir (NF). Means of means  $\pm$  SEM of  $n = 6$  independent biological replicates, 58–60 optical fields per condition. Number of puncta normalized to area of neuronal soma. Holm-Šídák multiple unpaired t-tests, \* $p$  < 0.05. **H** Immunoblot analysis of endogenous S2P levels in cortical neurons treated with vehicle (DMSO) or bortezomib (BTZ) obtained over  $n = 5$  biological replicates, normalized to  $\beta$ -actin. Same membranes as analyzed in Fig. 1 D and F.

its levels in the nucleus and found that BtdCPU treatment for 5 h resulted not in an increased but instead a significant reduction of CREB3L2 levels in the nucleus (Fig. 4C). To investigate this finding further, we performed a time course experiment and observed that BtdCPU had an effect on CREB3L2 levels in whole cell lysates of cortical neurons only after 60 minutes of treatment (Fig. 4D). Together, our findings identify that HRI activation positively regulates levels of ATF4, but sustained activation reduces levels of CREB3L2.

#### CREB3L2 levels are primarily regulated by proteasome-dependent degradation

A possible explanation for the seemingly contradictory finding that HRI activation results in increased ATF4 expression but decreases CREB3L2 levels, might be that CREB3L2 gets rapidly degraded via the ubiquitin-proteasome pathway [21]. To distinguish between the effects of proteasome inhibition and HRI activation, we measured the effect of proteasome inhibition on CREB3L2 and ATF4 levels in neurons expressing shCtrl or shHRI. Levels for both transcription factors were significantly increased in the BTZ conditions (Fig. 5A). The knockdown of HRI did not significantly change the increase for either transcription factor. Collectively, these findings reveal that levels of CREB3L2 are controlled by proteasome-dependent degradation, while sustained HRI activity is negatively correlated with CREB3L2 levels.

#### HRI activation prevents CREB3L2-ATF4 signaling effects

Because HRI negatively regulates CREB3L2 levels, we reasoned that activation of HRI during A $\beta$ <sub>42</sub>-induced stress might rescue some of the CREB3L2-ATF4 effects. To directly test this possibility, we applied BtdCPU to A $\beta$ <sub>42</sub>-treated neurons. Using PLA, we found that BtdCPU abolished the A $\beta$ <sub>42</sub>-dependent increase in the number of CREB3L2-ATF4 heterodimers in the nuclei of cortical neurons (Fig. 5B). CREB3L2 levels were significantly reduced in control and A $\beta$ <sub>42</sub>-treated neurons co-treated with BtdCPU, while ATF4 levels significantly increased in either condition (Fig. 5C). A transcriptional effect of CREB3L2-ATF4 signaling is the reduction of SNX3 expression, a component of the retromer complex [6]. Activation of HRI in A $\beta$ <sub>42</sub>-treated neurons prevented this effect and instead reverted SNX3 expression to baseline levels (Fig. 5C). These findings suggest that HRI activation by BtdCPU prevents the A $\beta$ <sub>42</sub>-induced accumulation of the ATF4-CREB3L2 heterodimer and its associated transcriptional effects.

#### DISCUSSION

Here, we report that the formation of the AD-linked transcription factor heterodimer CREB3L2-ATF4 is downstream of the inhibition of the proteasome by oligomeric A $\beta$ <sub>42</sub>. The finding that eIF2 $\alpha$  phosphorylation in the absence of proteasome inhibition is

insufficient to induce CREB3L2-ATF4, led us to investigate the role of the eIF2 $\alpha$ -kinase HRI, which can be activated by proteasome inhibition. ATF4 levels were increased by BTZ-treatment even in the context of HRI knockdown. While this finding is formally in line with the notion that BTZ could activate other eIF2 $\alpha$  kinases, prior work has identified HRI as the primary kinase mediating proteasome inhibition-dependent eIF2 $\alpha$  [14, 16]. We found that CREB3L2 is negatively regulated by sustained, i.e., longer than 60 minutes activation of HRI. Importantly, we did not observe a reduction in CREB3L2 with shorter times of HRI activation, leaving the possibility open that short-term activation of HRI or HRI activation in the context of proteasome inhibition can induce CREB3L2 levels. The fact that levels of both CREB3L2 and the heterodimer were reduced with HRI activation suggests that the amount of available CREB3L2 might be rate-limiting for heterodimer formation. These findings are compatible with a model in which both ATF4 and CREB3L2 are translated downstream of HRI, but in the absence of proteasome inhibition, CREB3L2 is rapidly degraded, and either no heterodimer is formed or it is unstable. In this model, the reduction of CREB3L2 levels under prolonged HRI activity would be part of a self-limiting stress response. This safeguarding mechanism fails in neurons exposed to A $\beta$ <sub>42</sub>, in a situation where eIF2 $\alpha$  phosphorylation and proteasome inhibition coincide.

The mechanisms by which direct, prolonged activation of HRI lowers levels of CREB3L2 while proteasome inhibition results in increased levels of CREB3L2 remain to be explored. Our finding that proteasome inhibition increases S2P levels and S2P-dependent release of CREB3L2 from the ER neurons suggests that this step might be involved in preventing the rapid degradation of CREB3L2.

In conclusion, we set out to elucidate the signaling pathways responsible inducing the AD-specific transcription factor complex, CREB3L2-ATF4, in response to soluble oligomeric A $\beta$ <sub>42</sub>. Our results establish that A $\beta$ <sub>42</sub> inhibits the proteasome, resulting in increased levels of both transcription factors in the nucleus. We provide evidence that the eIF2 $\alpha$ -kinase HRI regulates levels of ATF4 and CREB3L2 differently, where prolonged HRI activation results in increased levels of ATF4 and decreased levels of CREB3L2. However, with proteasome inhibition, which can activate the HRI-eIF2 $\alpha$  axis, levels CREB3L2 are increased as well. This data, along with previous literature suggests that CREB3L2 levels are usually kept low under normal physiological conditions due to basal level of HRI activity [16], then under proteasome inhibition, CREB3L2 levels increase because of lack of degradation and possibly through increased levels of the protease responsible for producing active CREB3L2. In response to soluble oligomeric A $\beta$ <sub>42</sub>, the effects of proteasome inhibition on CREB3L2 and heterodimer levels outweigh those of simple HRI activity. However, the overactivation of HRI in neurons

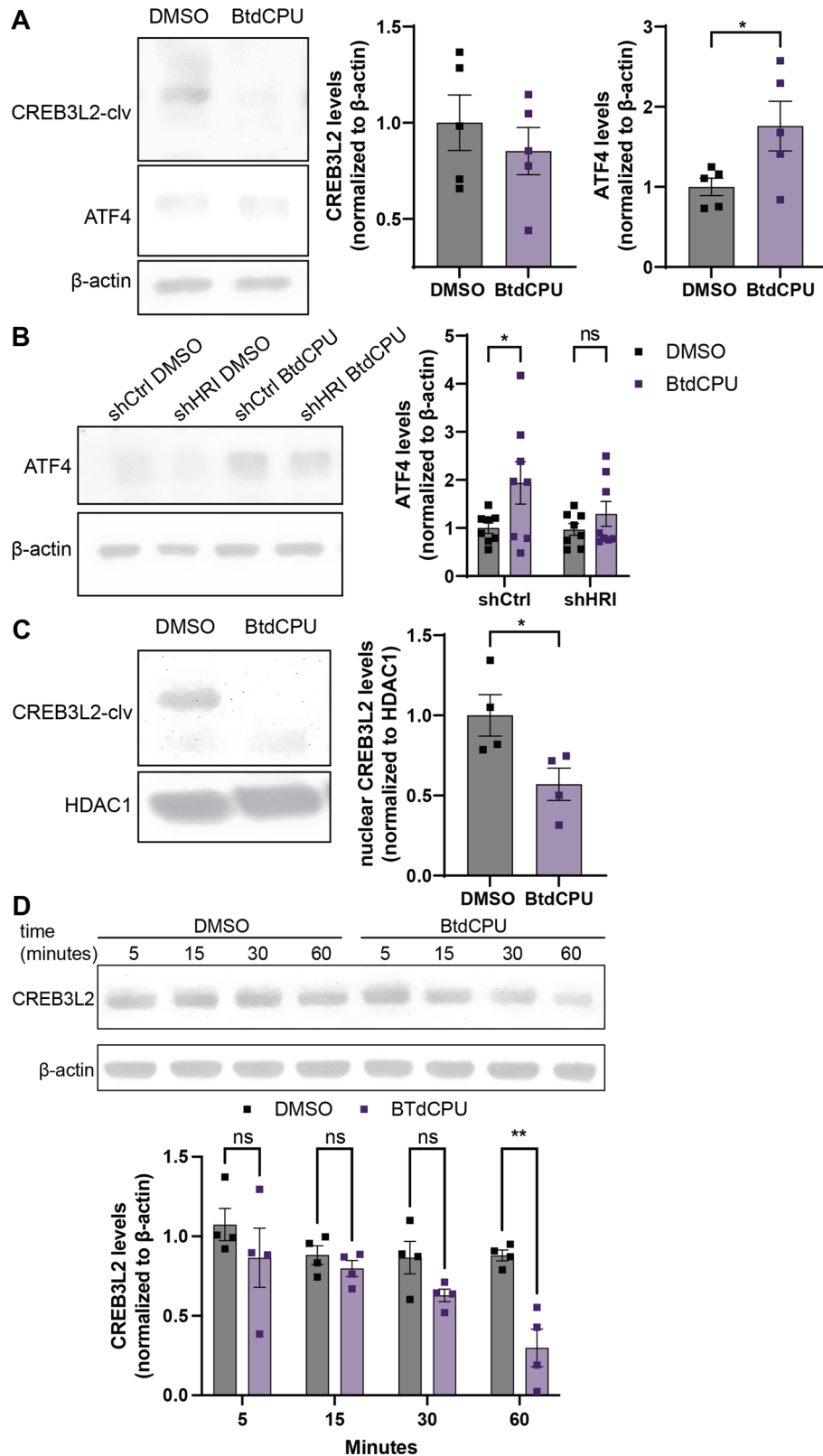


**Fig. 4 Long-term HRI activation negatively regulates CREB3L2 levels.** **A** Immunoblot analysis of CREB3L2 and ATF4 protein levels in whole cell lysates of vehicle (DMSO)- or BtdCPU-treated cortical neurons. Means  $\pm$  SEM of  $n = 5$  independent biological replicates, normalized to  $\beta$ -actin. Unpaired, two-tailed t-test;  $*p < 0.05$ . Same membranes as analyzed in Fig. 1 D and F. **B** Immunoblot analysis of ATF4 levels in vehicle (DMSO) or BtdCPU-treated cortical neurons transduced with either shCtrl or shHRI. Means  $\pm$  SEM of  $n = 8$  independent biological replicates. Holm-Šidák multiple unpaired t-tests;  $*p < 0.05$ . **C** Immunoblot analysis of nuclear CREB3L2 levels in vehicle (DMSO)- or BtdCPU-treated cortical neurons. Means  $\pm$  SEM of  $n = 4$  biological replicates, normalized to HDAC1. Unpaired, two-tailed t-test;  $*p < 0.05$ . **D** Time course analysis of CREB3L2 expression in cortical neurons treated with DMSO or BtdCPU. Means  $\pm$  SEM of  $n = 4$  independent biological replicates. Holm-Šidák multiple unpaired t-tests;  $**p < 0.01$ .

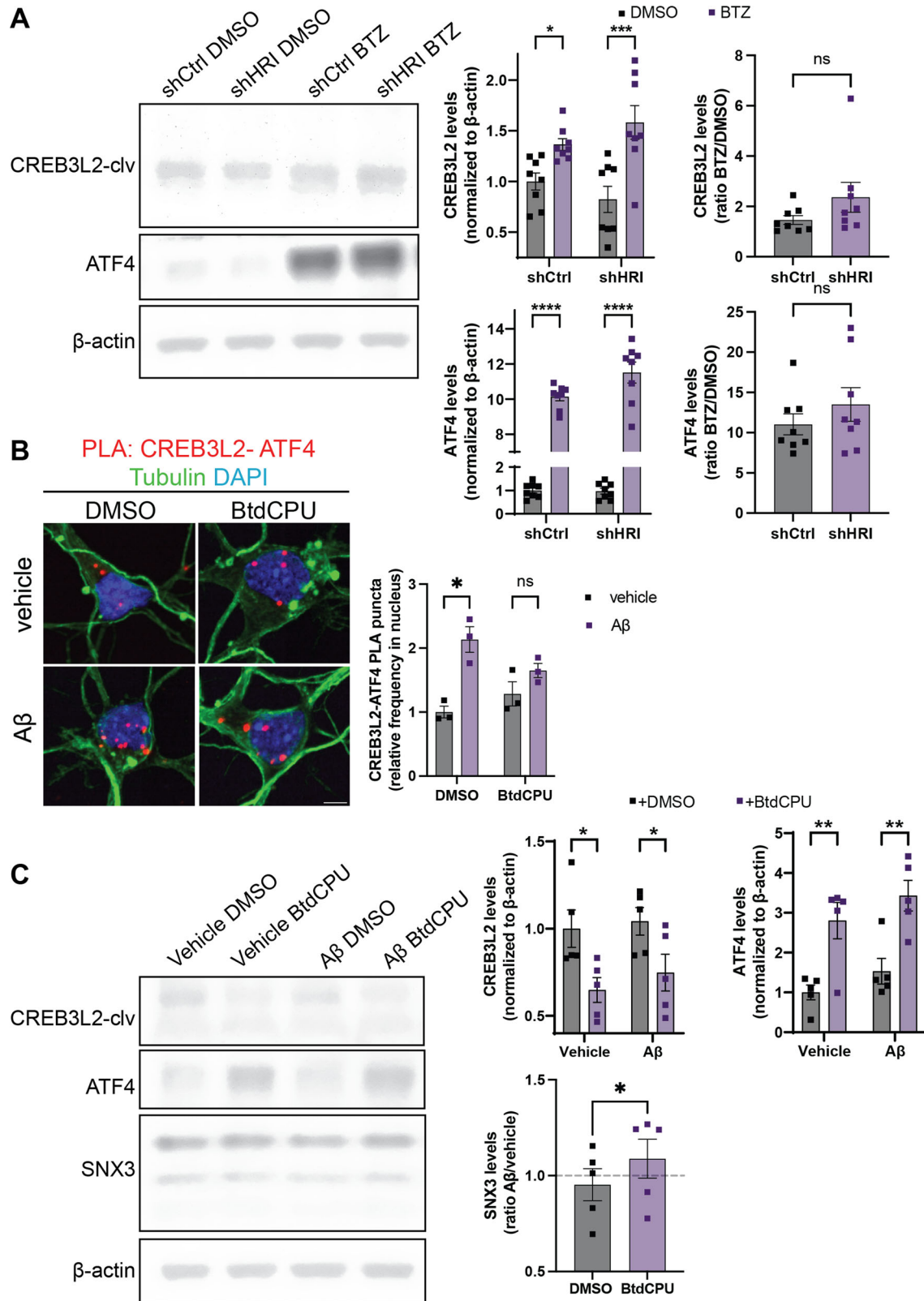


**Fig. 5 HRI activation interferes with CREB3L2-ATF4 signaling.** **A** Immunoblot analysis of CREB3L2 and ATF4 in vehicle (DMSO) or bortezomib (BTZ)-treated cortical neurons transduced with either shCtrl or shHRI. Means  $\pm$  SEM of  $n = 8$  independent biological replicates. Two-way ANOVA;  $*p < 0.05$ ,  $***p < 0.001$ . ATF4 and CREB3L2 ratios of BTZ- to DMSO- treated samples in shCtrl compared to shHRI for each trial. **B** PLA of CREB3L2-ATF4 in cortical neurons treated with DMSO or BtdCPU and A $\beta_{42}$  or vehicle for 8 h. Means of means  $\pm$  SEM of  $n = 3$  independent biological replicates, 62–70 optical fields per condition for nuclear ATF4-CREB3L2 events. Holm-Sídák multiple unpaired t-tests,  $*p < 0.05$ . Scale bar, 5  $\mu$ m. **C** Immunoblot analysis of CREB3L2, ATF4, and SNX3 in whole cell lysates of cortical neurons treated with vehicle or A $\beta_{42}$  in the presence of DMSO or BtdCPU. Means  $\pm$  SEM of  $n = 5$  independent biological replicates. Holm-Sídák multiple unpaired t-tests;  $*p < 0.05$ ,  $**p < 0.01$ . SNX3 ratios of A $\beta_{42}$ - over vehicle-exposed neurons compared between DMSO- and BtdCPU-treated. Paired t-test, two-tailed.  $*p < 0.05$ .

treated with A $\beta$ <sub>42</sub> can counteract some of the heterodimer-dependent transcriptional changes. These data suggest activation of HRI during the accumulation of misfolded proteins/proteasome inhibition as a potential approach to correct gene expression changes in response to A $\beta$ <sub>42</sub>.

## DATA AVAILABILITY

The data supporting the findings of this study are available from the corresponding author upon reasonable request.

## REFERENCES

- Jack CR Jr, Bennett DA, Blennow K, Carrillo MC, Dunn B, Haeblerlein SB, et al. NIA-AA Research Framework: Toward a biological definition of Alzheimer's disease. *Alzheimers Dement*. 2018;14:535–62.
- Jack CR Jr, Bennett DA, Blennow K, Carrillo MC, Feldman HH, Frisoni GB, et al. A/T/N: An unbiased descriptive classification scheme for Alzheimer disease biomarkers. *Neurology*. 2016;87:539–47.
- Miller JA, Oldham MC, Geschwind DH. A systems level analysis of transcriptional changes in Alzheimer's disease and normal aging. *J Neurosci*. 2008;28:1410–20.
- Gouveia Roque C, Phatnani H, Hengst U. The broken Alzheimer's disease genome. *Cell Genom*. 2024;4:100555.
- Baleriola J, Walker CA, Jean YY, Cray JF, Troy CM, Nagy PL, et al. Axonally synthesized ATF4 transmits a neurodegenerative signal across brain regions. *Cell*. 2014;158:1159–72.
- Gouveia Roque C, Chung KM, McCurdy EP, Jagannathan R, Randolph LK, Herline-Killian K, et al. CREB3L2-ATF4 heterodimerization defines a transcriptional hub of Alzheimer's disease gene expression linked to neuropathology. *Sci Adv*. 2023;9:eadd2671.
- Walker CA, Randolph LK, Matute C, Alberdi E, Baleriola J, Hengst U. Abeta(1-42) triggers the generation of a retrograde signaling complex from sentinel mRNAs in axons. *EMBO Rep*. 2018;19:e45435.
- Small SA, Kent K, Pierce A, Leung C, Kang MS, Okada H, et al. Model-guided microarray implicates the retromer complex in Alzheimer's disease. *Ann Neurol*. 2005;58:909–19.
- Seaman MN. The retromer complex - endosomal protein recycling and beyond. *J Cell Sci*. 2012;125:4693–702.
- Dey S, Baird TD, Zhou D, Palam LR, Spandau DF, Wek RC. Both transcriptional regulation and translational control of ATF4 are central to the integrated stress response. *J Biol Chem*. 2010;285:33165–74.
- Kondo S, Saito A, Hino S, Murakami T, Ogata M, Kanemoto S, et al. BBF2H7, a novel transmembrane bZIP transcription factor, is a new type of endoplasmic reticulum stress transducer. *Mol Cell Biol*. 2007;27:1716–29.
- Costa-Mattioli M, Walter P. The integrated stress response: From mechanism to disease. *Science*. 2020;368:eaat5314.
- Burwick N, Aktas BH. The eIF2-alpha kinase HRI: a potential target beyond the red blood cell. *Expert Opin Ther Targets*. 2017;21:1171–7.
- Yerlikaya A, Kimball SR, Stanley BA. Phosphorylation of eIF2alpha in response to 26S proteasome inhibition is mediated by the haem-regulated inhibitor (HRI) kinase. *Biochem J*. 2008;412:579–88.
- Yerlikaya A, DoKudur H. Investigation of the eIF2alpha phosphorylation mechanism in response to proteasome inhibition in melanoma and breast cancer cells. *Mol Biol*. 2010;44:859–66.
- Alvarez-Castelao B, Tom Dieck S, Fusco CM, Donlin-Asp P, Perez JD, Schuman EM. The switch-like expression of heme-regulated kinase 1 mediates neuronal proteostasis following proteasome inhibition. *Elife* 9, (2020)
- White MC, Schroeder RD, Zhu K, Xiong K, McConkey DJ. HRI-mediated translational repression reduces proteotoxicity and sensitivity to bortezomib in human pancreatic cancer cells. *Oncogene*. 2018;37:4413–27.
- Ramos-Fernandez E, Tajés M, Ill-Raga G, Vargas L, Busquets-García A, Bosch-Morato M, et al. Glutamatergic stimulation induces GluN2B translation by the nitric oxide-Heme-Regulated eIF2alpha kinase in cortical neurons. *Oncotarget*. 2016;7:58876–92.
- Ill-Raga G, Tajés M, Busquets-García A, Ramos-Fernandez E, Vargas LM, Bosch-Morato M, et al. Physiological control of nitric oxide in neuronal BACE1 translation by Heme-regulated eIF2alpha Kinase HRI induces Synaptogenesis. *Antioxid Redox Signal*. 2015;22:1295–307.
- Frank CL, Ge X, Xie Z, Zhou Y, Tsai LH. Control of activating transcription factor 4 (ATF4) persistence by multisite phosphorylation impacts cell cycle progression and neurogenesis. *J Biol Chem*. 2010;285:33324–37.
- Kondo S, Hino SI, Saito A, Kanemoto S, Kawasaki N, Asada R, et al. Activation of OASIS family, ER stress transducers, is dependent on its stabilization. *Cell Death Differ*. 2012;19:1939–49.
- Stine WB Jr, Dahlgren KN, Krafft GA, LaDu MJ. In vitro characterization of conditions for amyloid-beta peptide oligomerization and fibrillogenesis. *J Biol Chem*. 2003;278:11612–22.
- Carpenter AE, Jones TR, Lamprecht MR, Clarke C, Kang IH, Friman O, et al. CellProfiler: image analysis software for identifying and quantifying cell phenotypes. *Genome Biol*. 2006;7:R100.
- Harding HP, Novoa I, Zhang Y, Zeng H, Wek R, Schapira M, et al. Regulated translation initiation controls stress-induced gene expression in mammalian cells. *Mol Cell*. 2000;6:1099–108.
- Kondo S, Saito A, Asada R, Kanemoto S, Imaizumi K. Physiological unfolded protein response regulated by OASIS family members, transmembrane bZIP transcription factors. *IUBMB Life*. 2011;63:233–9.
- Axten JM, Medina JR, Feng Y, Shu A, Romeril SP, Grant SW, et al. Discovery of 7-methyl-5-(1-[3-(trifluoromethyl)phenyl]acetyl-2,3-dihydro-1H-indol-5-yl)-7H-pyrrolo[2,3-d]pyrimidin-4-amine (GSK2606414), a potent and selective first-in-class inhibitor of protein kinase R (PKR)-like endoplasmic reticulum kinase (PERK). *J Med Chem*. 2012;55:7193–207.
- Jiang HY, Wek RC. Phosphorylation of the alpha-subunit of the eukaryotic initiation factor-2 (eIF2alpha) reduces protein synthesis and enhances apoptosis in response to proteasome inhibition. *J Biol Chem*. 2005;280:14189–202.
- Keller JN, Hanni KB, Markesbery WR. Impaired proteasome function in Alzheimer's disease. *J Neurochem*. 2000;75:436–9.
- Thibaudeau TA, Anderson RT, Smith DM. A common mechanism of proteasome impairment by neurodegenerative disease-associated oligomers. *Nat Commun*. 2018;9:1097.
- Keck S, Nitsch R, Grune T, Ullrich O. Proteasome inhibition by paired helical filament-tau in brains of patients with Alzheimer's disease. *J Neurochem*. 2003;85:115–22.
- Almeida CG, Takahashi RH, Gouras GK. Beta-amyloid accumulation impairs multivesicular body sorting by inhibiting the ubiquitin-proteasome system. *J Neurosci*. 2006;26:4277–88.
- Tseng BP, Green KN, Chan JL, Blurton-Jones M, LaFerla FM. Abeta inhibits the proteasome and enhances amyloid and tau accumulation. *Neurobiol Aging*. 2008;29:1607–18.
- Park CW, Jung BK, Ryu KY. Reduced free ubiquitin levels and proteasome activity in cultured neurons and brain tissues treated with amyloid beta aggregates. *Mol Brain*. 2020;13:89.
- Oh S, Hong HS, Hwang E, Sim HJ, Lee W, Shin SJ, et al. Amyloid peptide attenuates the proteasome activity in neuronal cells. *Mech Ageing Dev*. 2005;126:1292–9.
- Zhao X, Yang J. Amyloid-beta peptide is a substrate of the human 20S proteasome. *ACS Chem Neurosci*. 2010;1:655–60.
- Lopez Salon M, Pasquini L, Besio Moreno M, Pasquini JM, Soto E. Relationship between beta-amyloid degradation and the 26S proteasome in neural cells. *Exp Neurol*. 2003;180:131–43.
- McCurdy EP, Chung KM, Benitez-Agosto CR, Hengst U. Promotion of Axon growth by the secreted end of a transcription factor. *Cell Rep*. 2019;29:363–377.e365.
- Guan M, Fousek K, Chow WA. Nelfinavir inhibits regulated intramembrane proteolysis of sterol regulatory element binding protein-1 and activating transcription factor 6 in castration-resistant prostate cancer. *FEBS J*. 2012;279:2399–411.
- Abdel-Nour M, Carneiro LAM, Downey J, Tsalikis J, Outlioua A, Prescott D, et al. The heme-regulated inhibitor is a cytosolic sensor of protein misfolding that controls innate immune signaling. *Science*. 2019;365:eaaw4144.
- Mukherjee T, Ramaglia V, Abdel-Nour M, Bianchi AA, Tsalikis J, Chau HN, et al. The eIF2alpha kinase HRI triggers the autophagic clearance of cytosolic protein aggregates. *J Biol Chem*. 2021;296:100050.
- Chen T, Ozel D, Qiao Y, Harbinski F, Chen L, Denoyelle S, et al. Chemical genetics identify eIF2alpha kinase heme-regulated inhibitor as an anticancer target. *Nat Chem Biol*. 2011;7:610–6.

## ACKNOWLEDGEMENTS

We thank members of the Hengst laboratory for helpful discussions; U.H. was supported by the NIH (R01NS109607, R01NS121337) and the BrightFocus Foundation (A20210305); M.M.P. was supported by the NIH (T32NS064928); C.G.R. was supported by the Alzheimer's Association (AARF-17-533511-RAPID); E.P.M. was supported by the NSF.

## AUTHOR CONTRIBUTIONS

KH-K and UH conceived and designed the experiments; KH-K, MMP, JEL, MAZ, CGR, EPM, and KMC performed the experiments and analyzed the data; KH-K and UH wrote the article with input from all authors.

## COMPETING INTERESTS

The authors declare no competing interests.

## ETHICS APPROVAL AND CONSENT TO PARTICIPATE

All methods were performed in accordance with the relevant guidelines and regulations. The use of animals for this study was evaluated and approved by the Institutional Animal Care and Use Committee (IACUC) of Columbia University (protocol AC-AABO8554).

## ADDITIONAL INFORMATION

**Supplementary information** The online version contains supplementary material available at <https://doi.org/10.1038/s41419-025-07586-0>.

**Correspondence** and requests for materials should be addressed to Ulrich Hengst.

**Reprints and permission information** is available at <http://www.nature.com/reprints>

**Publisher's note** Springer Nature remains neutral with regard to jurisdictional claims in published maps and institutional affiliations.



**Open Access** This article is licensed under a Creative Commons Attribution 4.0 International License, which permits use, sharing, adaptation, distribution and reproduction in any medium or format, as long as you give appropriate credit to the original author(s) and the source, provide a link to the Creative Commons licence, and indicate if changes were made. The images or other third party material in this article are included in the article's Creative Commons licence, unless indicated otherwise in a credit line to the material. If material is not included in the article's Creative Commons licence and your intended use is not permitted by statutory regulation or exceeds the permitted use, you will need to obtain permission directly from the copyright holder. To view a copy of this licence, visit <http://creativecommons.org/licenses/by/4.0/>.

© The Author(s) 2025